Nuclear data generation using machine learning

Hiroki IWAMOTO[†1]

[1]Nuclear Science and Engineering Center, Japan Atomic Energy Agency
[†]Email: iwamoto.hiroki@jaea.go.jp

Gaussian processes are used as a Bayesian machine learning technique to solve regression and classification problems. This paper reviews this technique, and presents some merits and issues for the nuclear data generation.

1 Introduction

Gaussian processes [1, 2] are used as a Bayesian machine learning technique to solve the regression and classification problems. Because a regression model based on Gaussian processes (GPR) gives predictive distributions for regression problems, this technique may be a powerful tool not only for evaluating nuclear data but also for determining the corresponding uncertainty. In the previous study, a method to generate nuclear data from experimental data was proposed based on GPR [3], and it was demonstrated that our method can generate reasonable regression curves and their uncertainties from experimental data. This paper reviews this technique, and some merits and issues for the nuclear data generation are presented.

2 Gaussian process regression

Suppose that we have N measured data points (measurement energy points $\boldsymbol{x}_N \in \mathbb{R}^N$ and corresponding cross sections with uncertainties [one standard deviation, 1σ], $\boldsymbol{t}_N \pm \delta\boldsymbol{t}_N \in \mathbb{R}^N$) for a certain nuclear reaction and that we aim to generate a set of cross-sections for certain M energy points $\boldsymbol{x}_M \in \mathbb{R}^M$. GPR expresses the conditional probability distribution of $\boldsymbol{t}_M \in \mathbb{R}^M$ given by $\boldsymbol{t}_N$, $p(\boldsymbol{t}_M|\boldsymbol{t}_N)$, as a Gaussian distribution with mean $\boldsymbol{\mu}_M$ and covariance $\boldsymbol{\Sigma}_{M,M}$:

$$p(\boldsymbol{t}_M|\boldsymbol{t}_N) = \mathcal{N}(\boldsymbol{t}_M \mid \boldsymbol{\mu}_M, \boldsymbol{\Sigma}_{M,M}), \tag{1}$$

$$\boldsymbol{\mu}_M = \mathbf{C}_{NM}^\top \mathbf{C}_{NN}^{-1} \boldsymbol{t}_N, \tag{2}$$

$$\boldsymbol{\Sigma}_{MM} = \mathbf{C}_{MM} - \mathbf{C}_{NM}^\top \mathbf{C}_{NN}^{-1} \mathbf{C}_{NM}. \tag{3}$$

The (i, j)-th element of the covariance $\mathbf{C}_{NN}$ is expressed as

$$C(\boldsymbol{x}_i, \boldsymbol{x}_j) = k(\boldsymbol{x}_i, \boldsymbol{x}_j) + \delta t_i \delta_{ij} \delta t_j, \tag{4}$$

where $k(\boldsymbol{x}_i, \boldsymbol{x}_j)$ represents the kernel function, and the δ_{ij} is the Kronecker delta. The (i, j)-th elements of $N \times M$ matrix $\mathbf{C}_{NM}$, $M \times N$ matrix $\mathbf{C}_{MN} (= \mathbf{C}_{NM}^\top)$, and $M \times M$ matrix $\mathbf{C}_{MM}$ are of the form:

$$C(\boldsymbol{x}_i, \boldsymbol{x}_j) = k(\boldsymbol{x}_i, \boldsymbol{x}_j). \tag{5}$$

For the kernel function, this study used the following radial basis function:

$$k(\boldsymbol{x}_i, \boldsymbol{x}_j) = \theta_1 \exp\left(-\frac{\theta_2}{2}||\boldsymbol{x}_i - \boldsymbol{x}_j||^2\right), \tag{6}$$

where $\boldsymbol{\Theta} = (\theta_1, \theta_2)$ is a set of hyperparameters, which is optimized by finding a solution that maximizes the marginal log likelihood $p(\boldsymbol{t}_N|\mathbf{C}_{NN}, \boldsymbol{\Theta})$:

$$\boldsymbol{\Theta}_{\text{opt}} = \underset{\boldsymbol{\Theta}}{\text{argmax}} \ln p(\boldsymbol{t}_N|\mathbf{C}_{NN}, \boldsymbol{\Theta}) \tag{7}$$

$$= \underset{\boldsymbol{\Theta}}{\text{argmax}} \left(-\frac{1}{2}\ln|\mathbf{C}_{NN}| - \frac{1}{2}\boldsymbol{t}_N\mathbf{C}_{NN}^{-1}\boldsymbol{t}_N^\top - \frac{N}{2}\ln(2\pi)\right). \tag{8}$$

3 Generated cross-sections

3.1 Nuclide-production cross-sections

Figure 1 compares the generated nuclide production cross-sections for the ^{27}Al$(p, X)^4$He and ^{27}Al$(p, X)^{10}$Be reactions with physics models of INCL++/ABLA07 [4, 5] and INCL4.6/GEM [6, 7] and evaluated nuclear data libraries of ENDF/B-VIII.0 [8], JENDL-4.0/HE [9], and TENDL-2019 [10]. The experimental data, which were measured with the activation method, were taken from the experimental nuclear database, EXFOR [11]. The blue dashed line with uncertainty band indicates the cross-sections generated by GPR. Although the physics models and evaluated nuclear data account for the trends of the production cross-sections as a function of incident energy, it fails to agree with the experimental data. These discrepancies would be solved by improving the phyicis model or model parameters. In contrast, since GPR draws smooth curves to fit the experimental data without the need for physics models, the curves agree in principle with the experiments.

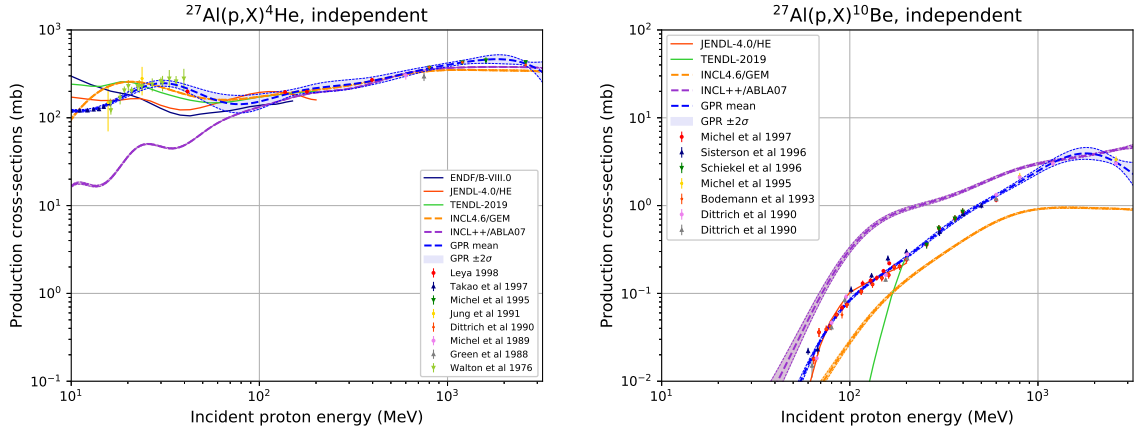

Figure 1: Comparisons of nuclide production cross-sections for the ^{27}Al$(p, X)^4$He reaction (left panel) and the ^{27}Al$(p, X)^{10}$Be reaction. (right panel) with physics models of INCL++/ABLA07 [4, 5] and INCL4.6/GEM [6, 7] and evaluated nuclear data libraries of ENDF/B-VIII.0 [8], JENDL-4.0/HE [9], and TENDL-2019 [10]. The dashed blue line and the light blue band present the mean of the generated predictive distribution and $\pm 2\sigma$ about the mean, respectively. The experimental data were taken from EXFOR [11].

3.2 GPR as a random sampler

Figure 2 shows generated nuclide-production cross-section for the $^{\mathrm{nat}}\mathrm{N}(p, X)^{10}\mathrm{Be}$ reaction and the generated correlation matrix. In the left panel of Figure 2, the 10 colored lines indicate random samples of the cross sections, which can be easily generated according $\boldsymbol{t}_M|\boldsymbol{t}_N \sim \mathcal{N}(\boldsymbol{t}_M \mid \boldsymbol{\mu}_M, \boldsymbol{\Sigma}_{MM})$. These random samples would be of significant benefit to subsequent uncertainty propagation analyses by the random sampling technique in research fields such as neutronics, reactor physics, and shielding analyses.

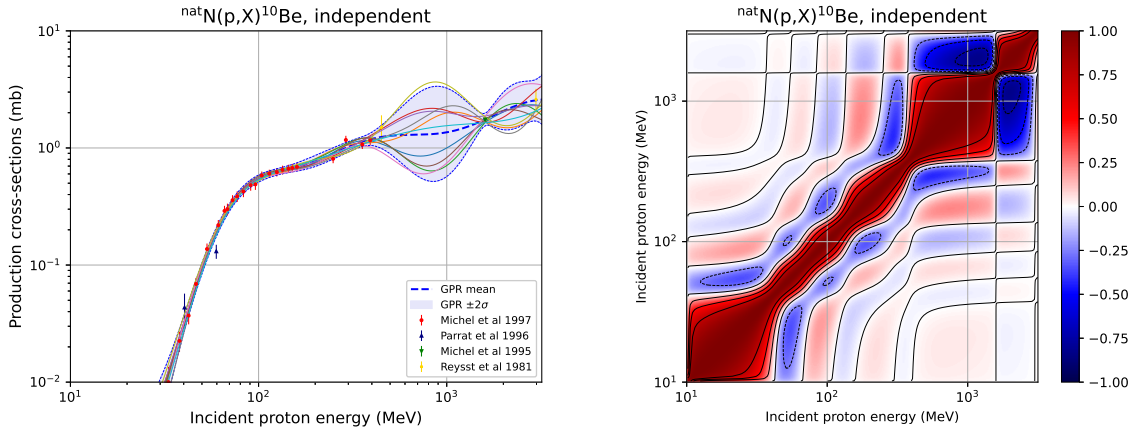

Figure 2: Generated nuclide-production cross-section (left panel) and the generated correlation matrix (right panel) for the $^{\mathrm{nat}}\mathrm{N}(p, X)^{10}\mathrm{Be}$ reaction. For the left panel, the dashed blue line and the light blue band present the mean of the generated predictive distribution and $\pm 2\sigma$ about the mean, respectively. The 10 colored lines present random samples generated according to $\boldsymbol{t}_M|\boldsymbol{t}_N \sim \mathcal{N}(\boldsymbol{t}_M \mid \boldsymbol{\mu}_M, \boldsymbol{\Sigma}_{MM})$. The experimental data were taken from EXFOR.

3.3 Case of small experimental dataset

Figure 3 illustrates the nuclide-production cross-section for the $^{27}\mathrm{Al}(p, pn)^{26}\mathrm{Al}$ reaction. In the left panel, the cross-section was generated from the experimental data by Sisterson, et al. [12] and Schneider, et al. [13]. Here, since the threshold energy can be deduced from the mass of the reaction system ($x_{\mathrm{th}} = 11.3$ MeV), it was considered as training data (i.e. $\{x_{\mathrm{th}}, t_{\mathrm{th}}, \delta t_{\mathrm{th}}\} = \{11.3\ \mathrm{MeV}, 10^{-3}\ \mathrm{mb}, 10^{-4}\ \mathrm{mb}\}$). Although its exact position including its uncertainty cannot be determined, a reasonable curve in this energy range seems to be obtained, and we confirmed that the generated uncertainty did not strongly depend on the additional training data. However, an unacceptably large uncertainty band is still observed at the GeV range, which is owing to the lack of experimental data. Such uncertainty information would be useful for motivating to conduct new experiments in terms of enhancing the prediction acuracy.

As one possible way to resolve such problems, it may be necessary to give some physical knowledge as training data. In this case, from the total proton-neutron cross-section systematics [14], the (p, pn) cross-sections in the GeV range is expected to be constant. In the right panel of Figure 3, auxiliary constant cross-section value points are added in the GeV range to take into account this knowledge. However, this ad hoc solution need to be improved in future.

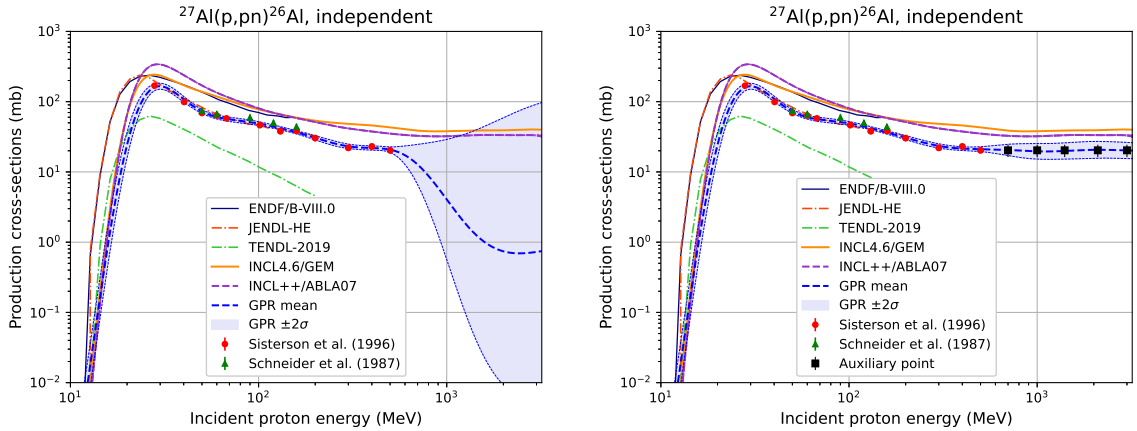

Figure 3: Left panel: nuclide production cross-section for the $^{27}\mathrm{Al}(p, pn)^{26}\mathrm{Al}$ reaction generated from the experimental data. Right panel: same as the left panel but with the inclusion of auxiliary points infered from the total proton-neutron cross-section systematics at the GeV range.

4 Summary

We have applied the GPR technique to generate nuclear data, focusing on proton-induced nuclide production cross-sections. Reasonable curves with corresponding uncertainties were obtained and the results indicate that this approach is effective for generating nuclear data.

References

[1] Rasmussen, C.F., Williams, C.K.I., Gaussian process for machine learning, The MIT press, Cambridge, 2006.

[2] Bishop, C.M., Pattern recognition and machine learning, Springer, New York, 2006.

[3] Iwamoto, H., Generation of nuclear data using Gaussian process regression, J. Nucl. Sci. Technol., vol.57, no.8, 2020, pp.932–938.

[4] Leray, S., et al., Extension of the Liège Intra Nuclear Cascade model to light ion-induced collisions for medical and space applications. J. Phys.: Conf. Series, vol.420, 2013, pp. 012065.

[5] Kelić, A., et al., ABLA07 – Towards a complete description of the decay channel of a nuclear system from spontaneous fission to multifragmentation. INDC(NDS)-0530, IAEA, 2008, pp.181–221.

[6] Boudard, A., et al., New potentialities of the Liège intranuclear cascade model for reactions induced by nucleons and light charged particles. Phys. Rev. C, 2013, 014606.

[7] Furihata, S., Statistical analysis of light fragment production from medium energy proton-induced reactions. Nucl. Instrum. Meth. B, vol.171, 2000, pp.251–258.

[8] Brown, D.A., ENDF/B-VIII.0: The 8$^{\mathrm{th}}$ major release of the nuclear reaction data library with CIELO-project cross sections, new standards and thermal scattering data. Nucl. Data Seets, vol.148, 2018, pp.1–142.

[9] Kunieda, S., et al., Overview of JENDL-4.0/HE and benchmark calculations. Proceedings of the 2015 Symposium on Nuclear Data, Tokai-mura, 2015, JAEA-Conf 2016-004, 2016, pp.44–46.

[10] Koning, A.J., et al., TENDL: Complete nuclear data library for innovative nuclear science and technology. Nucl. Data Sheets, vol.155, 2019, pp.1–55.

[11] Otuka, N., et al., Towards a more complete and accurate experimental nuclear reaction data library (EXFOR): International collaboration between nuclear reaction data centres (NRDC). Nucl. Data Sheets, vol.120, 2014, pp.272–276.

[12] Sisterson, J.M., et al., Measuring excitation functions needed to interpret cosmogenic nuclide production in lunar rocks. Conf. on Appl. of Accel. in Res. and Ind., Denton, USA, 1996, pp.811.

[13] Schneider, R.J., et al., Measurement of cross sections for aluminum-26 and sodium-24 induced by protons in aluminum. Nucl. Instrum. Meth. B, vol.29, 1987, pp.271–274.

[14] Cugnon, J., et al., Simple parametrization of cross-sections for nuclear transport studies up to the GeV range Nucl. Instrum. Meth. B, vol.111, 1996, pp.215–220.